NASA/TM—2004-213105 AIAA–2004–2983

Modeling of Turbulence Generated Noise in Jets

Abbas Khavaran
QSS Group, Inc., Cleveland, Ohio

James Bridges
Glenn Research Center, Cleveland, Ohio

June 2004

The NASA STI Program Office . . . in Profile

Since its founding, NASA has been dedicated to the advancement of aeronautics and space science. The NASA Scientific and Technical Information (STI) Program Office plays a key part in helping NASA maintain this important role.

The NASA STI Program Office is operated by Langley Research Center, the Lead Center for NASA's scientific and technical information. The NASA STI Program Office provides access to the NASA STI Database, the largest collection of aeronautical and space science STI in the world. The Program Office is also NASA's institutional mechanism for disseminating the results of its research and development activities. These results are published by NASA in the NASA STI Report Series, which includes the following report types:

- TECHNICAL PUBLICATION. Reports of completed research or a major significant phase of research that present the results of NASA programs and include extensive data or theoretical analysis. Includes compilations of significant scientific and technical data and information deemed to be of continuing reference value. NASA's counterpart of peer-reviewed formal professional papers but has less stringent limitations on manuscript length and extent of graphic presentations.

- TECHNICAL MEMORANDUM. Scientific and technical findings that are preliminary or of specialized interest, e.g., quick release reports, working papers, and bibliographies that contain minimal annotation. Does not contain extensive analysis.

- CONTRACTOR REPORT. Scientific and technical findings by NASA-sponsored contractors and grantees.

- CONFERENCE PUBLICATION. Collected papers from scientific and technical conferences, symposia, seminars, or other meetings sponsored or cosponsored by NASA.

- SPECIAL PUBLICATION. Scientific, technical, or historical information from NASA programs, projects, and missions, often concerned with subjects having substantial public interest.

- TECHNICAL TRANSLATION. English-language translations of foreign scientific and technical material pertinent to NASA's mission.

Specialized services that complement the STI Program Office's diverse offerings include creating custom thesauri, building customized databases, organizing and publishing research results . . . even providing videos.

For more information about the NASA STI Program Office, see the following:

- Access the NASA STI Program Home Page at ***http://www.sti.nasa.gov***

- E-mail your question via the Internet to help@sti.nasa.gov

- Fax your question to the NASA Access Help Desk at 301–621–0134

- Telephone the NASA Access Help Desk at 301–621–0390

- Write to:
  NASA Access Help Desk
  NASA Center for AeroSpace Information
  7121 Standard Drive
  Hanover, MD 21076

NASA/TM—2004-213105 AIAA–2004–2983

Modeling of Turbulence Generated Noise in Jets

Abbas Khavaran
QSS Group, Inc., Cleveland, Ohio

James Bridges
Glenn Research Center, Cleveland, Ohio

Prepared for the
Tenth Aeroacoustics Conference
cosponsored by the American Institute of Aeronautics and Astronautics
and the Confederation of European Aerospace Societies
Manchester, United Kingdom, May 10–12, 2004

National Aeronautics and
Space Administration

Glenn Research Center

June 2004

Acknowledgments

The authors would like to thank Dr. Marvin Goldstein and Dr. Stewart Leib from NASA Glenn Research Center for their helpful comments and suggestions.

Available from

NASA Center for Aerospace Information
7121 Standard Drive
Hanover, MD 21076

National Technical Information Service
5285 Port Royal Road
Springfield, VA 22100

Available electronically at http://gltrs.grc.nasa.gov

MODELLING OF TURBULENCE GENERATED NOISE IN JETS

Abbas Khavaran
QSS Group, Inc.
Cleveland, Ohio 44135

James Bridges
National Aeronautics and Space Administration
Glenn Research Center
Cleveland, Ohio 44135

A numerically calculated Green's function is used to predict jet noise spectrum and its far-field directivity. A linearized form of Lilley's equation governs the non-causal Green's function of interest, with the non-linear terms on the right hand side identified as the source. In this paper, contributions from the so-called self- and shear-noise source terms will be discussed. A Reynolds-averaged Navier-Stokes solution yields the required mean flow as well as time- and length-scales of a noise-generating turbulent eddy. A non-compact source, with exponential temporal and spatial functions, is used to describe the turbulence velocity correlation tensors. It is shown that while an exact non-causal Green's function accurately predicts the observed shift in the location of the spectrum peak with angle as well as the angularity of sound at moderate Mach numbers, at high subsonic and supersonic acoustic Mach numbers the polar directivity of radiated sound is not entirely captured by this Green's function. Results presented for Mach 0.5 and 0.9 isothermal jets, as well as a Mach 0.8 hot jet conclude that near the peak radiation angle a different source/Green's function convolution integral may be required in order to capture the peak observed directivity of jet noise.

1. Introduction

THIS paper is motivated by an increasing demand on the aeroacoustics community to achieve new levels of accuracy in noise prediction in order to meet the stringent regulations set for aircraft noise reduction. Experimental observations of jet noise spectra and angularity for a wide range of shock-free operating conditions show that a bi-modal description best fits a typical spectrum. This has prompted many to propose a two-source generation mechanism. In the mid-angle range, jet noise is usually attributed to small-scale turbulence. Prediction schemes such as MGBK[1] or Tam and Auriault[2] scale the noise to 7/2 power of turbulence kinetic energy and use a Reynolds-averaged Navier-Stokes solution (RANS) to estimate the source strength and its spectral shape. The general shape of the spectrum and its roll-off at the high- and low ends of its frequency range depends on the proposed source model as well as the accuracy of the propagation filter, i.e., Green's Function (GF). The non-causal GF solution of interest may be obtained from the inhomogeneous Lilley's equation or directly from linearized Euler equations using numerical methods or some form of analytical approximation.

The second mechanism for sound generation is commonly attributed to the large-scale turbulent structures, which are considered as a superposition of instability modes of the mean flow. It has been shown that when the base flow is properly represented as a non-parallel jet, these waves grow in amplitude and then decay farther downstream. They become increasingly more efficient with jet speed, and at small angles from the downstream axis. A recent study[3] describes instability waves as a conduit that helps carry the sound from the source region to the far field rather than a separate source. This way, a two-component spectrum may be thought of as contributions from two completely different Green's functions acting on the same source.

The non-causal GF described in the present paper is derived from Lilley's equation. A good approximation to the base flow that is useful for jets and adopted here is a unidirectional transversely sheared mean flow. From a practical point of view, a locally parallel flow provides added numerical efficiency with minimal degradation in accuracy. Any deviation from a true spreading jet is usually limited to a small angle range close to the jet axis and well within the zone of silence where contribution from a causal GF is likely to dominate. Upon linearizing the Navier-Stokes equations about the base flow (for an ideal gas), the nonlinear terms are moved to the right-hand side to obtain the inhomogeneous Pridmore-Brown equation[4]. The right-hand side terms, all second-order in fluctuating variables, are now identified as source. Fluid viscosity and entropy fluctuations are considered to be relatively

unimportant in noise generation and are neglected compared to other source terms. Two of the three remaining sources are quadrupole in nature and are referred to as self- and shear-noise source terms. The third source has a dipole character and is associated with temperature fluctuations.

A physics-based modelling approach usually relies on averaged equations of motion. Statistical properties of noise sources as described by a two-point space-time correlation are entirely modeled. As such, any deficiency in the predictions should directly be linked to the underlying assumptions, i.e., the model functions or, possibly, the mean flow itself. Yet a successful model could prove extremely useful as a potential design tool in concept studies and in making trend predictions. In addition to the source description, the propagation filter needs to be accurate enough to capture refraction and shielding of sound for a wide range of frequencies, angles, and operating conditions. A review of some commonly used high-frequency asymptotic forms of the GF following the usual WKB methods and comparison with the numerical solution[5] demonstrates that these solutions generally remain accurate down to a Strouhal number of 0.5. However, the extension of the WKB solution to the more general jets with multiple turning points presents additional challenges and may require a numerical calculation of the near-field solution in order to satisfy the matching conditions.

The objective of this paper is to present the details of the source as well as the GF in a physics-based prediction approach. Analytical solution to intensity calculations using an exact GF is given in section 2. Section 3 shows the modelling of the two-point velocity correlations using an exponential form to describe both spatial and temporal functions. The general features of the 90° spectrum are addressed in section 4. A parametric study of the GF using a RANS-based mean flow is discussed in section 5. In particular, it is demonstrated that the mean flow could have an amplifying effect on radiated sound at certain observer angles and for certain source locations. More importantly, it is argued that regardless of the source definition used in the convolution integral, a non-causal GF, due to its sizable zone of silence, is incapable of capturing the observed directivity of high-speed jets at their peak radiation angle. Sample noise predictions for Mach 0.5, and 0.9 cold jets and a Mach 0.801 hot jet at a temperature ratio of 3.0 are presented in sections 6 and 7 and compared with data recently collected at the Small Hot Jet Acoustic Rig (SHJAR) at the NASA Glenn Research Center. Some concluding remarks are given in section 8 regarding the near-term needs for improving a physics-based prediction approach.

2. The Governing Equation

Lilley's third-order wave equation[6] may be linearized about a unidirectional transversely sheared mean flow

$$p = p_o = \text{constant}, \quad v_i = \delta_{i1} U(x_2, x_3), \quad T = T_o(x_2, x_3),$$

and rearranged to a form commonly referred to as the Pridmore-Brown[4] equation

$$L\Pi \equiv \frac{D}{Dt}\left(\frac{D^2\Pi}{Dt^2} - \frac{\partial}{\partial x_j}(c^2 \frac{\partial \Pi}{\partial x_j}) \right) + 2c^2 \frac{\partial U}{\partial x_j} \frac{\partial^2 \Pi}{\partial x_1 \partial x_j} = \Gamma . \tag{1}$$

Here Γ is the source, $\vec{x} \equiv (x_1, x_2, x_3)$ are the Cartesian coordinates and x_1 is in the stream-wise direction, p is pressure (i.e., $p \equiv p_o + p'$), $\Pi \equiv (1/\gamma)\ln(p/p_o)$, $c^2 = \gamma R T_o$ is the mean sound speed, and the convective derivative operator is

$$\frac{D}{Dt} \equiv \frac{\partial}{\partial t} + U \frac{\partial}{\partial x_1} .$$

When pressure fluctuations p' are small relative to mean pressure p_o, the dependent variable is approximated as $\Pi \cong p'/(\gamma p_o)$. Goldstein[7,8] carried out a second-order expansion of Eq. (1) and introduced a new dependent variable $\pi' \equiv \Pi + \Pi^2/2$ to show that

$$L\pi' = \frac{D}{Dt}\frac{\partial f_i}{\partial x_i} - 2\frac{\partial U}{\partial x_i}\frac{\partial f_i}{\partial x_1} \tag{2}$$

and $$f_i \equiv \frac{\partial (u_i u_j)}{\partial x_j} + (c^2)'\frac{\partial \Pi}{\partial x_i}, \tag{3}$$

where $u_i \equiv v_i - \delta_{i1}U$ denotes the velocity fluctuations. The source term (3) may be approximated as $f_i \cong \partial(u_i u_j)/\partial x_j$ once fluctuations in sound speed $(c^2)' = \gamma R(T - T_o)$ are neglected (a valid approximation when jet is isothermal). With the dependent variable approximated as $\pi' \cong \Pi$ (see Ref. 9 for the equation governing Π^2), Eq. (2) becomes

$$L\Pi \cong \frac{D}{Dt}\frac{\partial^2 (u_i u_j)}{\partial x_i \partial x_j} - 2\frac{\partial U}{\partial x_i}\frac{\partial^2 (u_i u_j)}{\partial x_1 \partial x_j}, \quad \Pi \cong \frac{p'}{\gamma p_o}. \tag{4}$$

The analysis presented here-on is based on Eq. (4). The two terms on the right side of the above equation are referred to as self- and shear-noise source terms, respectively.

2.1 Green's Function

A stationary point source with frequency ω and location $\vec{x}^s$ (superscript *s* denotes a source location) is considered in defining the GF

$$L(\mathbb{G}e^{-i\omega t}) = c_\infty^2 e^{-i\omega t}\delta(\vec{x} - \vec{x}^s). \tag{5}$$

Using an adjoint method[10], the far-field GF is given as

$$\mathbb{G}(\vec{x}, \vec{x}^s, \omega) = \frac{1}{4\pi\omega R} e^{ik(R - x_1^s \cos\theta)} \sum_{m=0}^{\infty} f_m(r^s, k, \theta)\cos m(\varphi - \varphi^s), \tag{6}$$

where (R, θ, φ) are the observer spherical coordinates, with radius *R* measured from jet exit centerline, polar angle θ measured from stream-wise jet axis, and azimuthal angle φ is measured in a span-wise plane. Wave number is defined as $k = \omega / c_\infty$ and $r \equiv R\sin\theta$. Function $f_m(r, k, \theta)$ is a solution to the second-order compressible Rayleigh operator subject to appropriate matching conditions at the jet boundary. The linear operator *L* also supports instability waves, which for a jet are the well- known Kelvin-Helmholtz instabilities. Reference 11 argues that these waves are suppressed if the governing equations are solved in a frequency domain and if a time-harmonic response is assumed.

For a source type $D/Dt[c_\infty^2 e^{-i\omega t}\delta(\vec{x} - \vec{x}^s)]$, representative of the self-noise term in (4), the GF is denoted as $\hat{\mathbb{G}}$, and is related to $\mathbb{G}$ as $\hat{\mathbb{G}} = -(i\omega + U\partial/\partial x_1^s)\mathbb{G}$, which upon using (6) becomes

$$\hat{\mathbb{G}} = -i\omega(1 - M^s\cos\theta)\mathbb{G}. \tag{7}$$

Here $M^s \equiv U(r^s)/c_\infty$ is the acoustic Mach number at the source location.

The GF of interest in jet noise is associated with a moving singularity with source frequency ω^s and convection velocity $\hat{i}U_c$. For self-noise we write

$$L(Ge^{-i\omega t}) = \frac{D}{Dt}\{c_\infty^2 e^{-i\omega^s t}\delta(x_1 - U_c t)\delta(\vec{x}_t - \vec{x}_t^s)\}. \tag{8}$$

Subscript *t* denotes a transverse location. The above GF is derived from (7) and a convolution integral as

$$G(\vec{x},\vec{x}^s,\omega)e^{-i\omega t}=\frac{1}{2\pi}\int_{\omega}d\omega\int_{\vec{y}}\int_{\tau}\hat{\mathbb{G}}(\vec{x},\vec{y},\omega)e^{-i\omega t}e^{-i(\omega^s-\omega)\tau}\delta(\vec{y}_t-\vec{x}_t^s)\delta(y_1-U_c\tau)d\tau d\vec{y}. \tag{9}$$

Integrating with respect to τ and $\vec{y}_t$ yields

$$G(\vec{x},\vec{x}^s,\omega)e^{-i\omega t}=\frac{1}{2\pi U_c}\int_{\omega}d\omega\int_{y_1}\hat{\mathbb{G}}(\vec{x};\vec{x}_t^s,y_1;\omega)e^{-i\omega t}e^{-i(\omega^s-\omega)y_1/U_c}dy_1. \tag{10}$$

Using $\hat{\mathbb{G}}$ from (7) and (6) into (10) and invoking the parallel flow assumption; the integration with respect to y_1 yields a delta function

$$\int_{y_1}e^{-iky_1\cos\theta}e^{-i(\omega^s-\omega)y_1/U_c}dy_1=2\pi\delta[-\frac{\omega}{U_c}(1-M_c\cos\theta)+\frac{\omega^s}{U_c}], \tag{11}$$

where $M_c=U_c/c_\infty$ is the convection Mach number.

Placing (11) in (10), the integration with respect to ω is readily carried out

$$G(\vec{x},\vec{x}^s,\omega)e^{-i\omega t}=\frac{-i}{4\pi R}\frac{(1-M^s\cos\theta)}{(1-M_c\cos\theta)}e^{\frac{-i\omega^s t}{1-M_c\cos\theta}}.e^{\frac{i\omega^s/c_\infty}{1-M_c\cos\theta}R}\sum_m f_m(r^s,\frac{\omega^s/c_\infty}{1-M_c\cos\theta},\theta)\cos m(\varphi-\varphi^s). \tag{12}$$

Upon relating source and observer frequencies through the Doppler factor

$$\omega=\frac{\omega^s}{1-M_c\cos\theta}, \tag{13}$$

the GF to Eq. (8) becomes

$$G(\vec{x},\vec{x}^s,\omega)=\frac{-i}{4\pi R}\frac{(1-M^s\cos\theta)}{(1-M_c\cos\theta)}e^{ikR}\sum_m f_m(r^s,k,\theta)\cos m(\varphi-\varphi^s). \tag{14}$$

Equation (14) indicates that the adjoint equation should be solved at the observer frequency even though the source is moving. In addition, it illustrates that for a convecting type source, the dependence of the GF on the axial source location is purely implicit, i.e., through the flow definition at the jet slice. Once the adjoint equation is solved for given values of observer angle θ, Strouhal number *St,* and mode number *m*, function f_m should be known at any arbitrary source locations r^s on the jet slice. Strouhal number is defined using exit diameter and jet exit velocity $St=\omega D/(2\pi U_J)$.

2.2 Multi-Pole Sources

The far-field spectral density may be expressed as integration with respect to the source volume $\vec{y}$ of sound spectral density per unit volume of turbulence

$$\overline{p^2}(\vec{x},\vec{y},\omega)=\int_{\vec{\xi}}\int_{-\infty}^{+\infty}G(\vec{x},\vec{y}-\vec{\xi}/2,\omega)G^*(\vec{x},\vec{y}+\vec{\xi}/2,\omega)R(\vec{y},\vec{\xi},\tau)e^{i\omega\tau}d\tau d\vec{\xi}. \tag{15}$$

Here $R(\vec{y},\vec{\xi},\tau)$ denotes a two-point fourth-order space-time correlation between source points $\vec{y}_1 = \vec{y} - \vec{\xi}/2$ and $\vec{y}_2 = \vec{y} + \vec{\xi}/2$ separated by time τ and space $\vec{\xi}$. In a compact eddy approximation, the variation of the GF within the source region is usually neglected and the product GG^* is approximated as square of the magnitude of the GF at the center of the correlation $\vec{y}$, and taken out of the above integral. The phase variation in the GF, however, could become a factor at high frequency when the eddy length scale exceeds the acoustic wavelength. The complex function f_m appearing in the series summation of Eq. (14) contains the phase information of the GF. To simplify the analysis, a form of the phase factor applicable in the high frequency limit is used here

$$\overline{p^2}(\vec{x},\vec{y},\omega) = \left|G(\vec{x},\vec{y},\omega)\right|^2 \int_{\vec{\xi}} \int_{-\infty}^{+\infty} e^{-i\vec{k}.\vec{\xi}} R(\vec{y},\vec{\xi},\tau) e^{i\omega\tau} d\tau d\vec{\xi}. \tag{16}$$

The above double integral, referred to as the wave-number frequency spectrum, may be expressed either in a fixed or a moving frame. In a convecting frame, $\vec{\xi}_m = \vec{\xi} - \hat{i}\, U_c \tau$, and $R(\vec{y},\vec{\xi},\tau) = R_m(\vec{y},\vec{\xi}_m,\tau)$, hence

$$\int_{-\infty}^{+\infty} e^{i\omega\tau} d\tau \int_{\vec{\xi}} R(\vec{y},\vec{\xi},\tau) e^{-i\vec{k}.\vec{\xi}} d\vec{\xi} \equiv \int_{-\infty}^{+\infty} e^{i\omega^s\tau} d\tau \int_{\vec{\xi}_m} R_m(\vec{y},\vec{\xi}_m,\tau) e^{-i\vec{k}.\vec{\xi}_m} d\vec{\xi}_m. \tag{17}$$

A spectral coefficient for a two-point fourth-order correlation of stress component $u_i u_j$ at points $\vec{y}$ and $\vec{y}'$ is defined as (prime designates separation in space and time)

$$I_{ijkl}(\vec{y},\omega^s) \equiv \int_{\vec{\xi}_m} \int_{-\infty}^{+\infty} \overline{(u_i u_j)(u_k' u_l')}\, e^{-i\vec{k}.\vec{\xi}_m} e^{i\omega^s\tau} d\tau d\vec{\xi}_m \quad , \tag{18}$$

and over-bar points to a time-averaged quantity. Equation (18) was written in a moving frame according to the right-hand side of (17). Presence of double derivatives operating on the source terms of equation (4) indicates that the appropriate GF should ultimately be calculated for a singularity type

$$\frac{D}{Dt}\{c_\infty^2 \frac{\partial^2}{\partial x_i \partial x_j} e^{-i\omega^s t} \delta(x_1 - U_c t)\delta(\vec{x}_t - \vec{x}_t^{\,s}) Q_{ij}\}. \tag{19}$$

The analysis may be carried out as described in the convolution integral leading to Eq. (9). However, the source spatial derivatives are now moved to the GF prior to $\vec{y}$ integration. For example, an application of $\partial^2 / \partial y_1 \partial y_1$ to $\hat{\mathfrak{G}}(\vec{x},\vec{y};\omega)$ in the integrand of Eq. (9) generates $(-ik\cos\theta)^2$ as seen from Eq. (6). Subsequently, $(k\cos\theta)^4$ multiplies sound intensity due to source correlation $\overline{(u_1 u_1)(u_1' u_1')}$. A derivative of $\hat{\mathfrak{G}}$ with respect to the span-wise source coordinates y_2 or y_3, acts on $f_m(r^s,k,\theta)\cos m(\varphi - \varphi^s)$. The algebra is quite lengthy but relatively straightforward. It may be shown that to the first order of approximation, quadrupoles of self noise, once integrated azimuthally for a ring volume within an axisymmetric jet, relate to the axial component I_{1111}. For an isotropic turbulence the result simplifies

$$(1 - M^s\cos\theta)^4 (\rho^s)^2 k^4 I_{1111}. \tag{20}$$

This, in view of (14), leads to the following expression for the sound spectral density per unit ring volume at radius r^s

$$\overline{p_{self}^2}(\vec{x},\vec{y},\omega) \cong \frac{1}{(4\pi R)^2} \frac{(1 - M^s\cos\theta)^6}{(1 - M_c\cos\theta)^2} \left(\frac{\rho^s}{\rho_\infty}\right)^2 (\rho_\infty^2 I_{1111}) k^4 \sum_m \left| f_m(r^s,k,\theta)\right|^2. \tag{21}$$

The above result is integrated over jet volume elements that radiate directly to the far field. Noise from sources internal to the jet requires special treatment due to reflection from solid boundaries. Goldstein and Leib[12] give an approximate high-frequency solution for sound emission due to internal mixing.

It will be shown in Sec. 7 that Eq. (14) scales like $\rho^{1/2}$ with jet density, hence sound spectral density in Eq. (21) scales with ρ^3.

3. Source Model

For simplicity we consider isotropic turbulence. The axial correlation coefficient needed in Eq. (21) is obtained from (18) when all indices are set equal to one. Using the usual quasi-normal approximation for the joint probability distribution of turbulence, a fourth-order correlation is written as a product of second-order tensors. In addition, a second-order correlation is written in a separable form

$$\overline{u_i u_j'}(\vec{\xi},\tau) = R_{ij}(\vec{\xi})h(\tau) \quad . \tag{22}$$

Appropriate modelling of a two-point velocity correlation is a crucial step in a physics-based prediction approach. For reasons discussed in Ref. 1 as supported by measurements[13,14], exponential functions are selected here to represent both spatial and temporal dependencies of the correlation

$$f(\xi_m) \equiv e^{-\pi\xi_m/\ell}, \qquad h(\tau) \equiv e^{-|\tau/\tau_o|}. \tag{23}$$

In (23), $\xi_m \equiv|\vec{\xi}_m|$ is measured in a moving frame, and is equivalent to $[(\xi_1 - U_c\tau)^2 + \xi_2^2 + \xi_3^2]^{1/2}$ if used in a fixed frame, and f is the scalar function that appears in the isotropic from of R_{ij}. Parameters ℓ and τ_o denote the length- and time-scales of the correlation

$$\ell \equiv c_\ell \kappa^{3/2} / \varepsilon, \qquad \tau_o \equiv c_\tau \kappa / \varepsilon \,. \tag{24}$$

Turbulence kinetic energy κ and its dissipation rate ε are usually provided through a RANS type solution and (c_ℓ, c_τ) represent a pair of calibration constants.

Using (22) in (18) shows that

$$I_{1111}(y,\omega^s) = 2H(\omega^s)\int_{\vec{\xi}_m} R_{11}^2(\vec{\xi}_m)e^{-i\vec{k}\cdot\vec{\xi}_m}d\vec{\xi}_m, \tag{25}$$

$$H(\omega^s) \equiv \int_{-\infty}^{+\infty} h^2(\tau)e^{i\omega^s\tau}d\tau. \tag{26}$$

Upon representing $R_{11}(\vec{\xi}_m)$ according to the homogeneous isotropic model of Batchelor[15] with f as defined in (23), it is shown[1] that

$$I_{1111}(\vec{y},\omega^s) = \frac{4}{5\pi^2}(\overline{u_1^2})^2\,\ell^3 H(\omega^s)N(k\ell). \tag{27}$$

Here $N(k\ell)$ denotes a non-compactness factor (Appendix A), which appears in the analysis due to the phase variation of the GF. As was discussed in Ref. 1, $N(k\ell)$ remains equal to 1.0 when $0 \le k\ell < 2\pi$, and decays rapidly as the eddy length-scale exceeds the wave-length of acoustic disturbances (i.e., $k\ell > 2\pi$).

Integrating Eq. (26) in conjunction with (23) results in

$$H(\omega^s) = \frac{\tau_o}{1+(\omega^s\tau_o/2)^2}. \tag{28}$$

Upon using (24) and (28) in (27) and replacing $\overline{u_1^2}$ with $2\kappa/3$

$$I_{1111}(\vec{y},\omega^s) = \frac{16}{45\pi^2}\left(\frac{c_\ell}{c_\tau}\right)^3 \kappa^{7/2} \frac{\tau_o^4}{1+(\omega^s \tau_o/2)^2} N(k\ell)\,. \tag{29}$$

Eq. (29) shows that sound intensity scales with $\kappa^{7/2}$. A third calibration constant A_m should multiply Eq. (29) to account for the fraction of turbulence kinetic energy converted to sound. This factor is combined with other constants preceding $\kappa^{7/2}$

$$I_{1111}(\vec{y},\omega^s) = A_m \kappa^{7/2} \frac{\tau_o^4}{1+(\omega^s \tau_o/2)^2} N(k\ell)\,. \tag{30}$$

Eq. (21) in conjunction with (30) is integrated over the jet volume (all rings within each slice) to calculate the far-field sound due to self-noise sources.

The appropriate GF for shear-noise source term is similar to Eq. (14), but divided by $\omega(1-M^s\cos\theta)$. Once the variations in dU/dr within the source correlation volume are neglected, the shear-noise spectral density due to a unit ring volume may be approximated as

$$\overline{p^2_{shear}}(\vec{x},\vec{y},\omega) \cong \frac{1}{(4\pi R)^2}\frac{\left(\frac{2dU/dr}{\omega}\right)^2}{(1-M_c\cos\theta)^2}\left(\frac{7}{2}\cos^2\theta\right)\left(\cos^2\theta + \frac{(1-M^s\cos\theta)^2}{c^2/c_\infty^2}\right) \times (\rho_\infty^2 I_{1111})k^4 \sum_m \left|f_m(r^s,k,\theta)\right|^2 . \tag{31}$$

This expression remains small at and near mid angles; however it generates significant directivity away from 90° as opposed to the self-noise spectrum, which is more omni-directional.
The coupling between self- and shear-noise terms is neglected in the following predictions.

4. Spectrum Function

The spectrum at 90°, also referred to as the master spectrum, is derived from product $k^4 H(\omega)N(k\ell)$ as seen from Eqs. (21) and (30). It takes the following form once turbulence correlation is modeled according to (23)

$$F(\omega\tau_o) \equiv \frac{(\omega\tau_o)^4}{1+(\omega\tau_o/2)^2} N(k\ell)\,. \tag{32}$$

In the absence of factor $N(k\ell)$, function $F(\omega\tau_o)$ becomes infinite like ω^2 as $\omega \to \infty$. On the other hand, with increasing ω the phase variation in the GF becomes increasingly significant as the eddy correlation length exceeds the acoustic wavelength. Thus spectral function $F(\omega\tau_o)$ decays at large frequency once factor $N(k\ell)$ is included (figure 1). This practically amounts to limited self-cancellation of high wave-number components of noise within the correlation. Also shown in this figure is the 90° spectrum function as calculated with temporal function $h(\tau) \equiv \exp[-\sqrt{(\sigma/2)^2 + (\tau/\tau_o)^2}]$. Proper selection of small constant σ would assure high-frequency decay even with factor $N(k\ell)$ selected as 1.0; however the spectrum becomes narrower. A Gaussian temporal function $\exp(-\tau^2/\tau_o^2)$ generates a relatively narrow spectral range due to its steep roll-off at high frequency and may not be a suitable model for jet noise prediction.

5. Numerical Evaluation of the Green's Function

In this section numerical calculation to the GF is presented for a range of parameters of common interest in jet noise prediction. A careful study of this non-causal GF and its association with the source location, frequency, and jet speed provides valuable insight into its contribution towards a total solution.

Equation (14), once normalized with respect to its free-space value, is integrated azimuthally to define ring source directivity

$$D^2(\vec{x},\vec{x}^s,\omega) \equiv \frac{(4\pi R)^2}{2\pi}\int_{-\pi}^{+\pi}\left|G(\vec{x},\vec{x}^s,\omega)\right|^2 d\varphi^s. \tag{33}$$

Both stationary and convecting type sources are considered. Source convection velocity is defined as a weighted average of local and exit velocities according to

$$U_c = 0.50U + 0.25U_j. \tag{34}$$

Alternative expressions[16] for U_c based on local, exit, and ambient jet velocities are available and could readily be tested. When the denominator of Eq. (14) becomes singular, the usual Ffowcs-Williams[17] correction is applied.

Mean flow predictions (RANS) were generated for a Mach 0.90 cold jet using WIND[18] flow solver available at the NASA Glenn Research Center. Source location $\vec{y}$ is identified through the ring radius r^s and its distance from jet exit x_1^s.

Directivity D for a stationary ring source at one diameter from jet exit, and for selected values of St from 0.10 to 5.0 is shown in figures 2a through 2d. It is observed that sources in the proximity of the jet centerline produce a larger directivity. The zone of silence grows noticeably in size with increasing frequency as expected. Figures 2c and 2d show that zone of silence may grow as large as 60^o (relative to the jet axis) for the more energetic segments of the jet, i.e., the jet mixing layer. Figures 3a through 3d use the flow definition at x_1^s=7.5D to highlight the significance of the jet profile on sound refraction. It is noted that source strength should ultimately multiply the GF when calculating the actual sound spectrum.

Source convection is known to amplify the radiated sound in the mean flow direction. This is illustrated in figures 4 and 5, which should be compared with the figures 2b and 3b for similar stationary sources.

6. Acoustic Results

Far-field spectra for Mach 0.50 and 0.90 cold jets were predicted on an arc R/D = 100, and compared with SHJAR data recently acquired at the NASA Glenn Research Center. Atmospheric attenuation has been removed from all measurements in order to make a lossless comparison with predictions. RANS solutions for the 2" diameter convergent nozzles were generated using the in-house WIND code with a standard $k\varepsilon$ turbulence model. Upstream nozzle conditions were specified in terms of plenum temperature ratio T_r and the pressure ratio.

Calibration constants c_τ, c_ℓ (see Eq. 24) and A_m (see Eq. 30) were set as 0.1846, 2.9430 and 1.2946 respectively. The argument of the non-compactness factor $k\ell = (c_\ell/c_\tau)(\omega\tau_o)(\kappa^{0.5}/c_\infty)$ is found to work better for a wide range of Mach numbers when divided by the local acoustic Mach number $U(r^s)/c_\infty$.

Figure 6 shows the spectra for Mach 0.50 cold jet at selected inlet angles. Self noise as well as total noise (i.e., self + shear) are plotted separately at each angle. Factor $(1-M^s\cos\theta)^6$ in the numerator of Eq. (21) works to produce an omni-directional appearance for self noise. The shift in spectral peak with angle shows good agreement with data. This behavior is primarily caused by the mean flow effect and is captured by the GF. Figure 7 shows similar comparisons for a Mach 0.90 cold jet. The agreements are generally very good, both in level as well as the spectral peak location.

Near the dominant radiation angle of the Mach 0.90 jet, differences start to emerge. The data points to a distinct spectral peak near 150^o inlet angle and at the Strouhal number of 0.20. It is suggested here that this peak is quite possibly influenced by the Kelvin-Helmhotz instabilities, which manifest themselves at high subsonic and supersonic Mach numbers. These waves dominate the distinct directivity of high speed jet noise at shallow angles, and their peak radiation frequency is sometimes scaled with Helmholtz number ($He \equiv f D/c_\infty$). As we will see shortly, addition of heat enhances this peak as the acoustic Mach number exceeds 1.0.

7. Hot Jets

An increase in the acoustic Mach number due to heat may cause the factor $(1 - M^s \cos\theta)$, appearing in the denominator in the adjoint Lilley equation, to become singular. The numerical integration should now continue along an appropriate path in the complex plane, and around the singularity[10]. A better illustration of the GF is, perhaps, given through

$$\Lambda(\vec{x},\vec{x}^s,\omega) \equiv (1 - M^s \cos\theta)(\rho^s / \rho_\infty)^{-0.5} D(\vec{x},\vec{x}^s,\omega) \tag{35}$$

where D^2 was defined in Eq. (33). The appearance of the density factor in Eq. (35) serves to demonstrate that the GF scales with the square root of density at moderate to high frequency. This is examined by observing the behavior of the GF at 90°.

Shown in figures 8a and 8b are the GF for a stationary ring source within a Mach 0.90 hot jet at a temperature ratio of T_r = 2.78. At this temperature the acoustic Mach number is supersonic (i.e., $U/c_\infty = 1.45$). Inspection of the GF at $\theta = 90^o$ and at *St* = 0.10 shows some dispersion with source location (see Fig. 8a). Figure 8b shows that the above density scaling is successful at *St* = 1.0. More importantly, this figure demonstrates that at mid- to high frequency, the GF in Eq. (14) scales like $(1 - M^s \cos\theta)^{-1}$ outside its zone of silence

It is also evident that, compared to a Mach 0.90 cold jet, the zone of silence has grown in size irrespective of the frequency (see figures 3a and 8a). The implications are that the above GF is not going to provide the required noise directivity near the peak radiation angle.

Figures 9a and 9b show similar results for a convecting ring source.

Figure 10 shows the jet noise spectrum at 90° for a 2" diameter, Mach 0.801, T_r =3.0 hot jet as calculated using an exact GF as well as a density-scaled GF (i.e., GF is simply set equal to $\rho^{1/2}/\rho_\infty^{1/2}$). The difference is fairly small and limited to the low frequency range.

The far-field spectra at *R/D* = 100 for this jet is also compared with recent SHJAR data as seen in figure 11. Let's consider the 90° spectrum, which stands 3 to 8 dB below measurements. This spectrum is entirely defined through Eq. (21) with $\theta = 90^o$. The preceding arguments demonstrate that sound spectral density scales like ρ^3, in addition to the usual $\kappa^{7/2}$ scaling. This implies that the mean density reductions caused by heat addition should be compensated for by a boost in turbulence in order to reach the required noise level. Choices available are quite clear: (a) additional noise sources due to heat; (b) adequate increase in turbulence level from heat; or some combination of (a) and (b).

Lighthill's formulation of the acoustic analogy shows that in the absence of the viscous stress tensor, source consists of an additional term $(p' - c_\infty^2 \rho')$. Once entropy fluctuations are neglected this becomes $(c^2 - c_\infty^2)\rho'$ which is not necessarily small compared to terms usually kept in the equation. Unfortunately ρ' now appears on both sides of the equation. Other forms of the analogy have tried, for example, new definitions for the dependent variable, in an effort to curtail the impact of those inconvenient terms that are usually neglected. In the current formulation, it is argued[7] that the second term on the right hand side of Eq. (3) is of the order of $(U/c)^2(u^2/\ell)$ relative to the first term that scales like (u^2/ℓ). For the present hot jet, the second term has a magnitude of 0.64 compared to the first, which makes it relatively significant. Modelling of this term, however, poses new difficulties due to the appearance of p' in the source.

In the latest formulation of the acoustic analogy, Goldstein[19] selects a new dependent variable, referred to as the generalized pressure, and writes the third-order wave equation in a form that does not include the dependent variable as part of the source.

Tam *et.al*[20] modified their $k\varepsilon$ turbulence model in order to improve their fine-scale predictions for hot jets. They proposed a new addition to the turbulent viscosity, as related to the mean density gradient, which accounts for enhanced mixing and increased growth of the shear layer when jets are hot. More recently[21], they modified their two-point space-time correlation model to increase its decay rate for hot jets. This new model, which takes advantage of four additional empirical parameters, provides improved prediction for hot jets at mid-angles.

Prediction of figure 11 defines turbulent viscosity[18] as $\nu_t = c_\mu \kappa^2/\varepsilon$, where $c_\mu = 0.09$. Shown in figure 12a is the predicted turbulence kinetic energy for the hot jet and comparison with the Particle Image Velocimetry (PIV) measurements[14]. Data clearly indicates a faster mixing as seen by the shorter core length and higher concentration of turbulence at the end of the core. A similar comparison for the Mach 0.90 cold jet (figure 12b) demonstrates better agreement, both in the length of the potential core as well as turbulence. It is quite likely that some form of modification to the two-equation turbulence model[22] could promote shear layer mixing at high temperatures and produce additional turbulence to improve our hot jet predictions at 90° and the nearby angles. In the vicinity of the peak radiation angle, instability related noise quickly overwhelms the hot jet solution as suggested by figure 11.

8. Concluding Remarks

This paper details some important features of the source as well as the propagation Green's function in a physics-based jet noise prediction methodology. A careful examination of the propagation filter in a locally parallel flow shows that the zone of silence grows increasingly large with jet velocity. It could encompass a sizeable region near the downstream jet axis as the acoustic Mach number becomes supersonic. Although non-parallel effects are known to reduce the low-frequency descent rate into the zone of silence[10], it is unlikely that at the peak directivity angle this Green's function could capture all contributions to the overall noise of high-subsonic or supersonic jets. A parallel flow assumption is expected to provide reliable prediction near the sideline angles, and to become effective in a broader angle range at lower jet speeds. The instability related noise, therefore, becomes the dominant source of jet noise in the vicinity of its peak radiation angle as the acoustic Mach number grows supersonic.

Our hot jet prediction confirms the need for some form of enhanced mixing or recalibration of the usual two-equation turbulence model for heated jets. However, the source term associated with temperature fluctuations in Eq. (3) remains a point of contention. The non-unique quality of the source in any analogy-type argument indicates that it might not be necessary to seek new sources to compensate for possible weaknesses in a RANS solution or the model representation of a two-point correlation.

Appendix A. Phase Variation of the Green's Function

When wavelength of the acoustic disturbances is small relative to the correlation length scale (i.e., $\lambda < \ell$), it is shown[1] that the axial correlation coefficient I_{1111} (defined in Eq. 25) consists of a non-compactness factor $N(k\ell)$ at high frequency. For example, when turbulence is isotropic, this factor becomes

$$N(k\ell) = 20\left(\frac{\pi}{k\ell}\right)^5\left[3\tan^{-1}\left(\frac{k\ell}{2\pi}\right) - 2\frac{k\ell}{\pi}\frac{5\left(\frac{k\ell}{\pi}\right)^2 + 12}{\left(\left(\frac{k\ell}{\pi}\right)^2 + 4\right)^2}\right], \quad \text{for} \quad f(\xi) = e^{-\pi\xi/\ell}, \tag{A1}$$

$$N(k\ell) = \exp\left(-\frac{k^2\ell^2}{8\pi}\right), \quad \text{for} \quad f(\xi) = e^{-\pi\xi^2/\ell^2}. \tag{A2}$$

References

[1]Khavaran, A., Bridges, J., and Freund, J. B., "A Parametric Study of Fine-Scale Turbulence Mixing Noise," AIAA Paper 2002-2419, June 2002.

[2]Tam, C. K. W., and Auriault, L., "Jet Mixing Noise from Fine-Scale Turbulence," AIAA Journal, **37(2)**, 1999.

[3]Goldstein, M. E., and Handler, L. M., "The Role of Instability Waves in Predicting Jet Noise," AIAA Paper 2003-3256, May 2003.

[4]Pridmore-Brown, D. C., "Sound Propagation in a Fluid Flowing Through an Attenuating Duct," J. Fluid Mechanics, **(4)**, pp. 393-406, 1958.

[5]Wundrow, D. W., and Khavaran, A., "On the Applicability of High-Frequency Approximation to Lilley's Equation," NASA/CR-2003-212089, 2003 (To appear in the J. Sound and Vibration, 2004).

[6]Lilley, G. M., "On the Noise from Jets, Noise Mechanisms,"AGARD-CP-131, pp. 13.1-13.12, 1974.

[7]Goldstein, M. E., "An Exact from of Lilley's Equation with a Velocity Quadrupole/Temperature Dipole Source Term," J. Fluid Mechanics, (**443)**, pp. 232-236, 2001.

[8]Goldstein, M. E., "Aeroacoustics of Turbulent Shear Flows," Ann. Rev. Fluid Mechanics, **(16),** pp. 262-295, 1984.

[9]Colonius, T., Lele, S. K., and Moin, P., "Sound Generation in a Mixing Layer," J. Fluid Mechanics, **(330)**, pp.375-409, 1997.

[10]Tam, C. K. W., and Auriault, L. "Mean Flow Refraction Effects on Sound Radiated from Localized Source in Jets," J. Fluid Mechanics, **(370)**, pp. 149-174, 1998.

[11]Agarwal A., Morris, P. J., and Mani, R., "Calculation of Sound Propagation in Nonlinear Flows: Suppression of Instability Waves," AIAA Journal, **42(1)**, January 2004.

[12]Goldstein, M. E., and Leib, S. J., "Emission of Sound from Turbulence Convected by a Parallel Mean Flow in the Presence of a Confining Duct," J. Sound and Vibration, **235(1)**, pp. 25-42, 2000.

[13]Bridges, J. and Wernet, M. P., "Turbulence Measurements of Separate Flow Nozzles with Mixing Enhancement Features," AIAA paper 2002-2484, June 2002.

[14]Bridges, J. and Wernet, M. P., "Measurements of the Aeroacoustic Sound Source in Hot Jets" AIAA paper 2003-3130, May 2003.

[15]Batchelor, G. K., *The Theory of Homogeneous Turbulence*, Cambridge Univ. Press, Cambridge, England, UK, 1960.

[16]Hunter, C. A., and Thomas, R. H., "Development of a Jet Noise Prediction Method for Installed Jet Configurations," AIAA Paper 2003-3169, 2003.

[17]Ffowcs-Williams, J. E., "The Noise from Turbulence Convected at High Speed," Phil. Transaction of the Royal Society of London, Series A, **(255)**, pp. 469-503, 1963.

[18]Bush, R. H., Power, G. D., and Towne, C. E., "WIND- The Prediction Flow Solver of the NPARC Alliance," AIAA Paper 1998-0935, 1998.

[19]Goldstein, M. E., "A Generalized Acoustic Analogy," J. Fluid Mechanics, (**488**), pp. 315-333, 2003.

[20]Tam, C. K. W., and Ganesan, A. "A Modified k-e Turbulence Model for calculating the Mean Flow and Noise of Hot Jets," AIAA Journal 42(1), January 2004.

[21]Tam, C. K. W., Pastouchenko, N. N., and Viswanathan, K., "Fine Scale Turbulence Noise from Hot Jets," AIAA Paper 2004-0362, January 2004.

[22]Abdol-Hamid, K. S., Pao, S. P., Massey, S. J., and Elmiligui, A., A., "Temperature Corrected Turbulence Model for High Temperature Jet Flow,"AIAA Paper, 2003-4070, 2003.

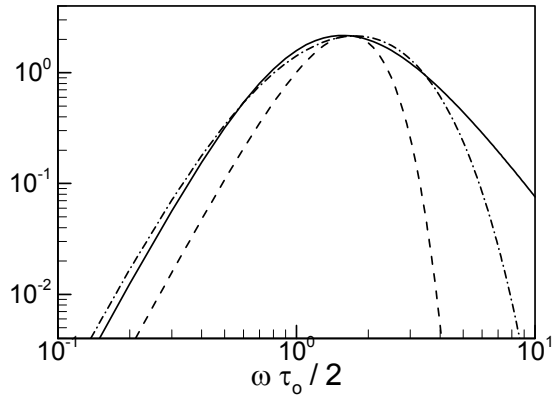

Fig. 1 Spectral shape function at 90° with temporal function defined as: $\exp(-|\tau/\tau_o|)$, solid line; $\exp\{-(0.4^2+\tau^2/\tau_o^2)^{0.50}\}$, dash-dot; $\exp(-\tau^2/\tau_o^2)$, dashed line.

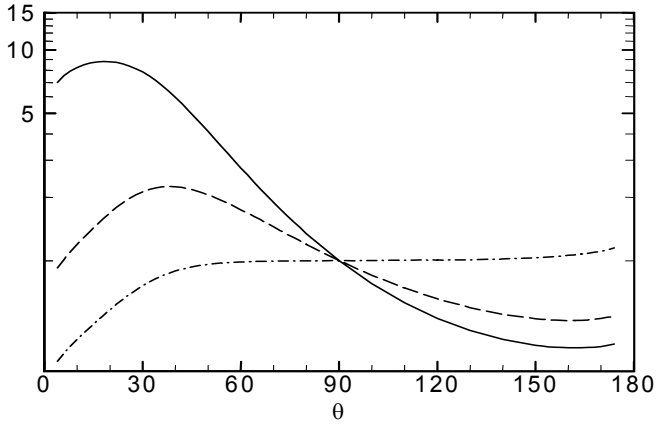

Fig. 2a Directivity $D(\vec{x},\vec{x}^{s},\omega)$ due to a stationary ring source within a Mach 0.9 cold jet at $St = 0.10$, x_1^s/D= 1.0 and r^s/D: 0.0 (solid line); 0.50 (dashed line); 1.0 (dash-dot).

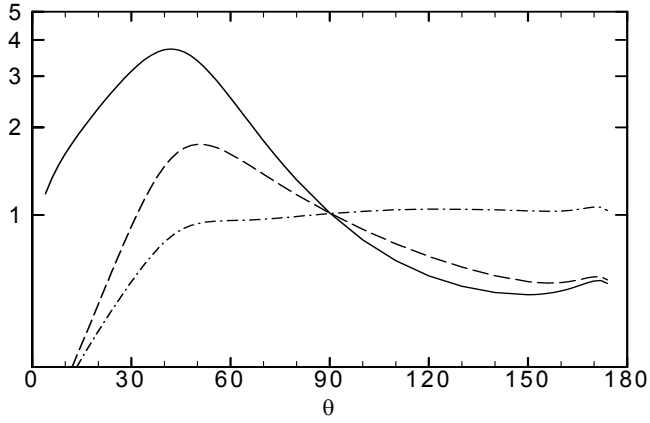

Fig. 2b As figure 2a but for St = 0.25.

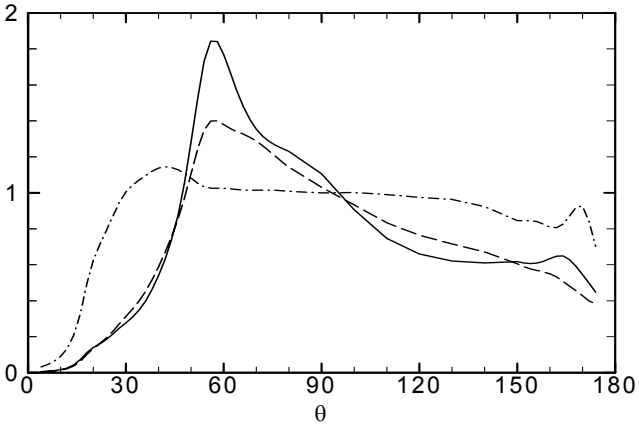

Fig. 2c As figure 2a but for St = 1.0.

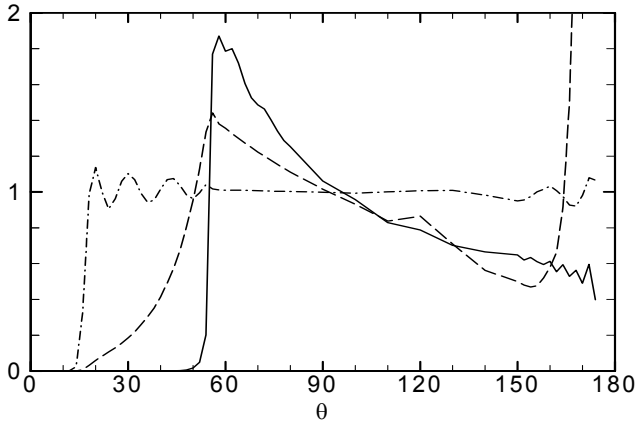

Fig. 2d As figure 2a but for St = 5.0.

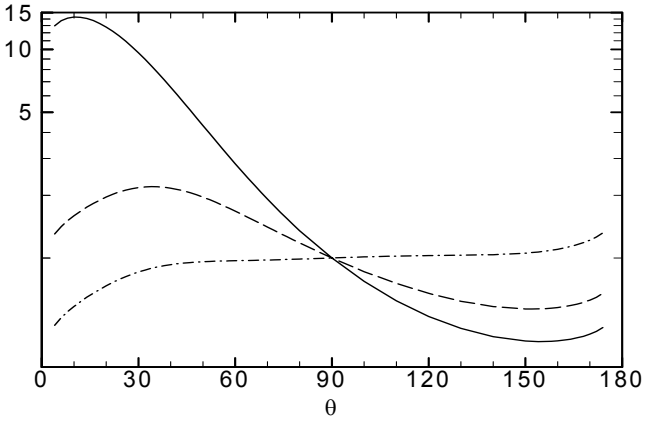

Fig. 3a Directivity $D(\vec{x},\vec{x}^{s},\omega)$ due to a stationary ring source within a Mach 0.9 cold jet at $St = 0.10$, x_1^s/D= 7.5 and r^s/D: 0.0 (solid line); 0.50 (dashed line); 2.0 (dash-dot).

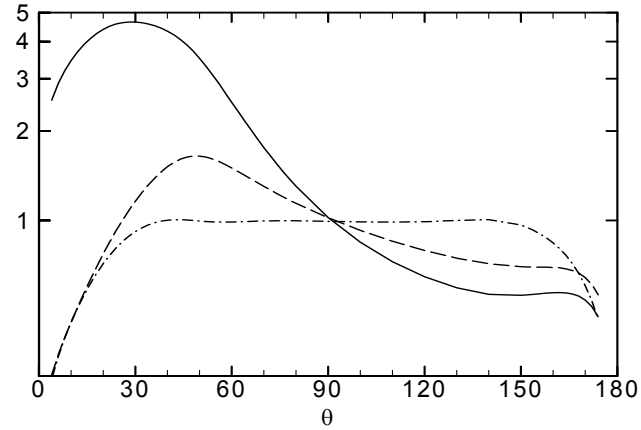

Fig. 3b As figure 3a but for St = 0.25.

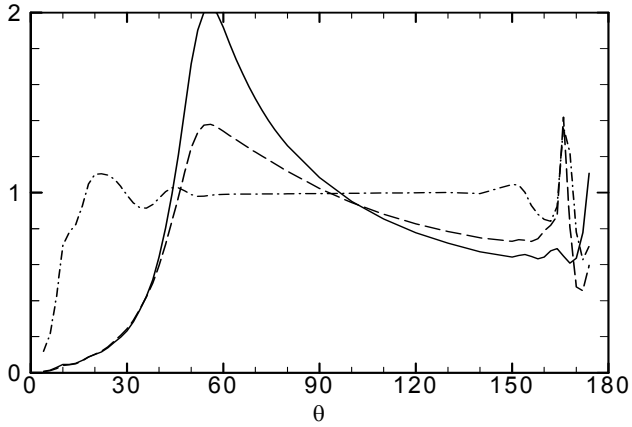

Fig. 3c As figure 3a but for St =1.0.

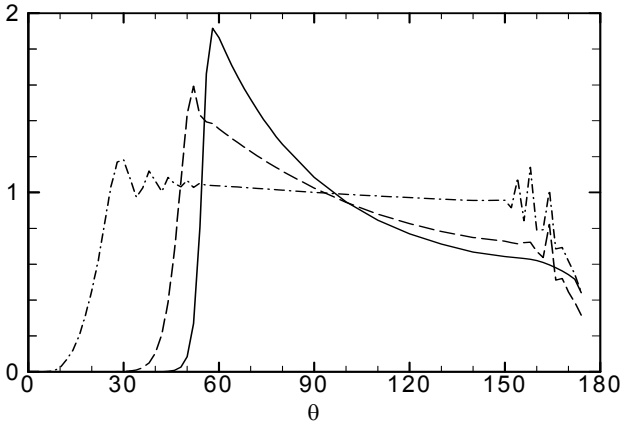

Fig. 3d As figure 3a but for St =5.0.

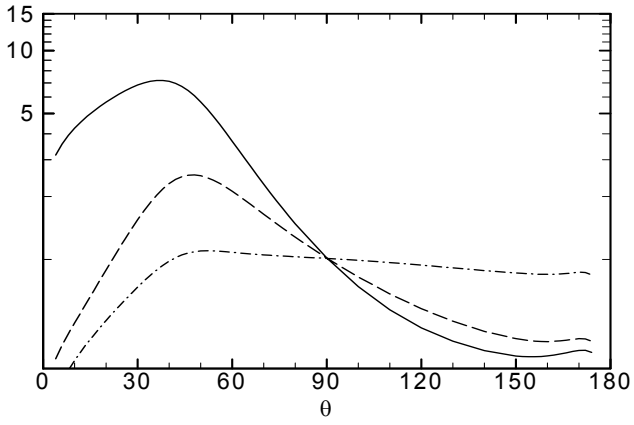

Fig. 4 Directivity $D(\vec{x},\vec{x}^{s},\omega)$ due to a convecting ring source within a Mach 0.9 cold jet at observer St = 0.25, x_1^s/D=1.0 and r^s/D: 0.0 (solid line); 0.50 (dashed line); 1.0 (dash-dot).

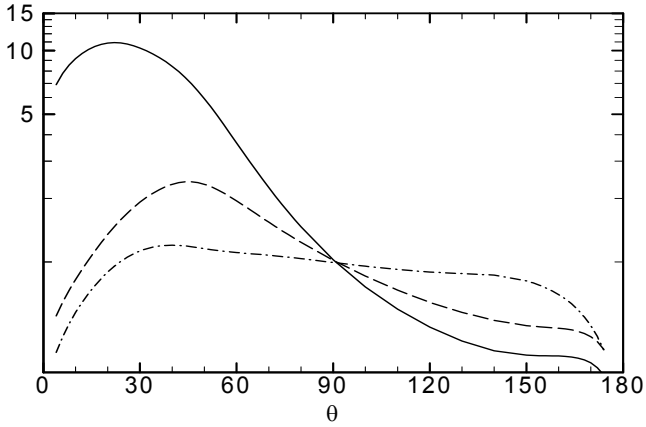

Fig. 5 As figure 4 but for a ring source at x_1^s/D=7.5 and r^s/D: 0.0 (solid line); 0.50 (dashed line); 2.0 (dash-dot).

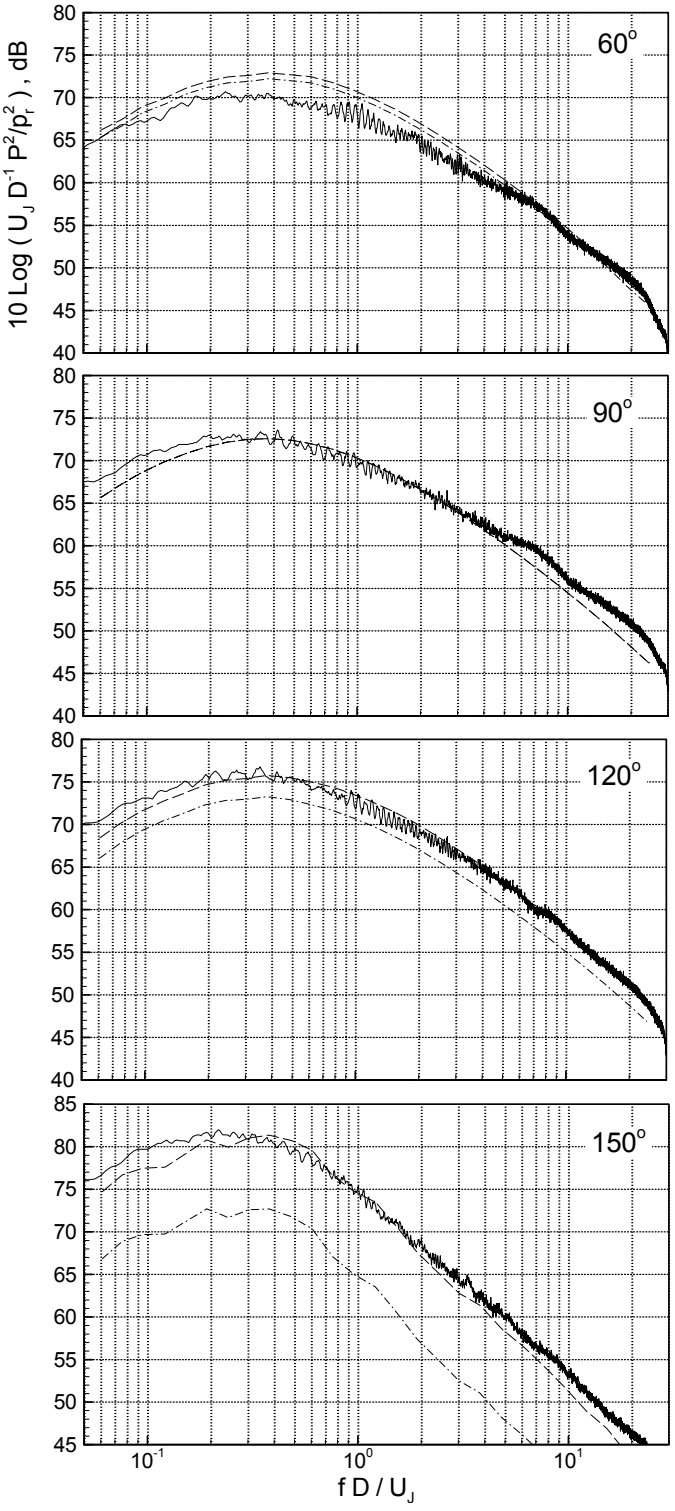

Fig. 6 Far field spectra for Mach 0.50, T_r =1.0 jet at indicated inlet angles and at R/D = 100. Self noise (dash-dot); Self + Shear noise (dashed line); data (solid line).

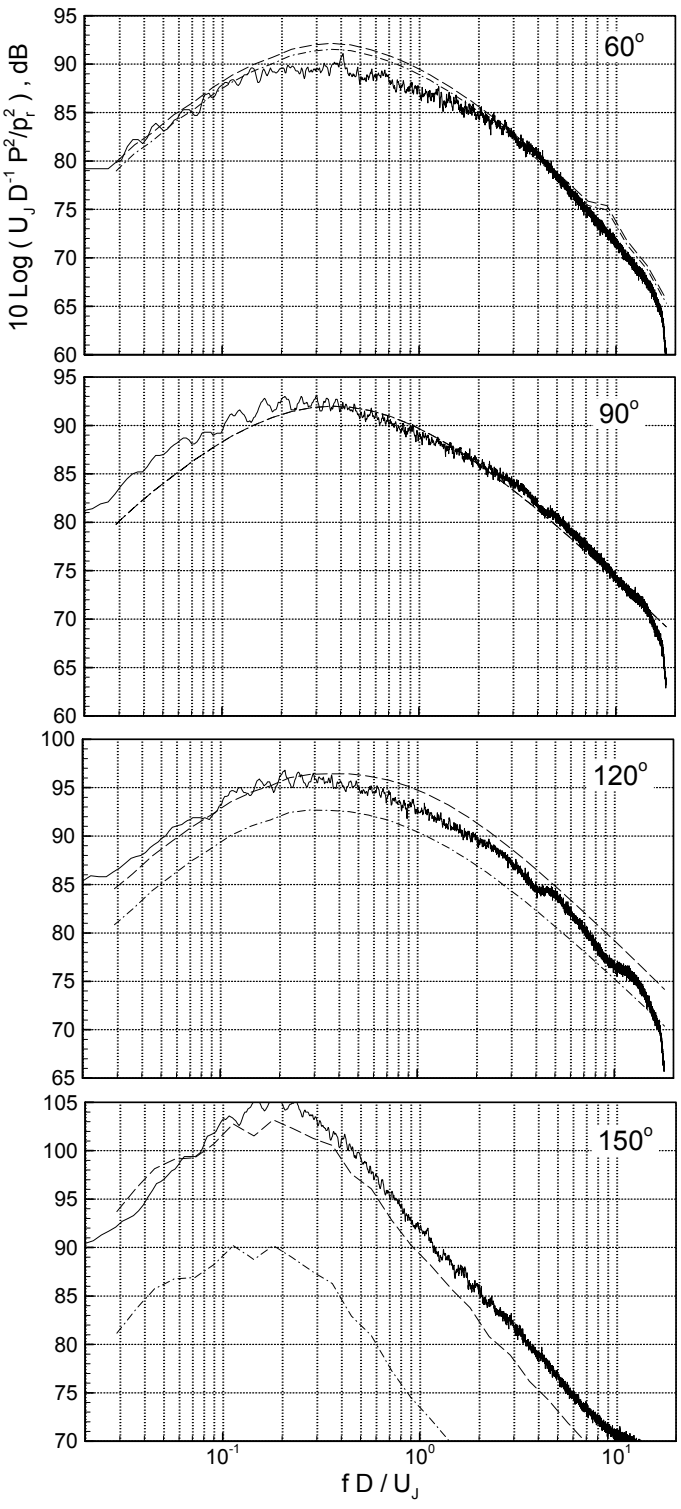

Fig. 7 Far field spectra for Mach 0.90, T_r =1.0 jet at indicated inlet angles and at R/D = 100. Self noise (dash-dot); Self + Shear noise (dashed line); data (solid line).

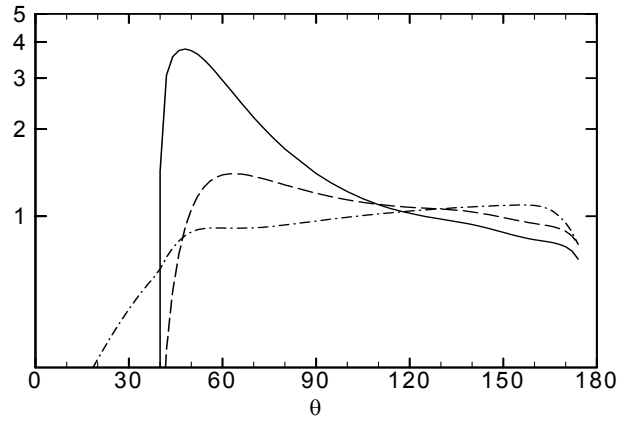

Fig. 8a Directivity $\Lambda(\vec{x},\vec{x}^{\,s},\omega)$ due to a stationary ring source within Mach 0.9, T_r=2.78 jet at St = 0.10, x_1^s/D=7.5 and r^s/D: 0.0 (solid line); 0.50 (dashed line); 2.0 (dash-dot).

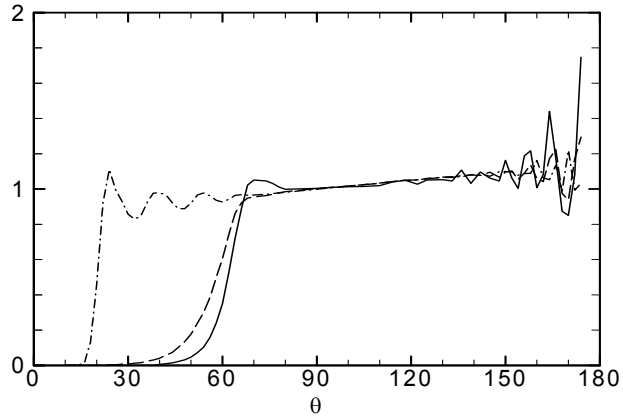

Fig. 8b As figure 8a but for a stationary ring source at St = 1.0.

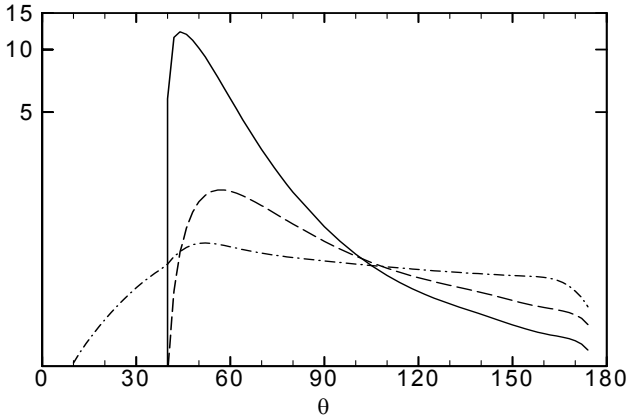

Fig. 9a As figure 8a but for a convecting ring source at observer St = 0.10.

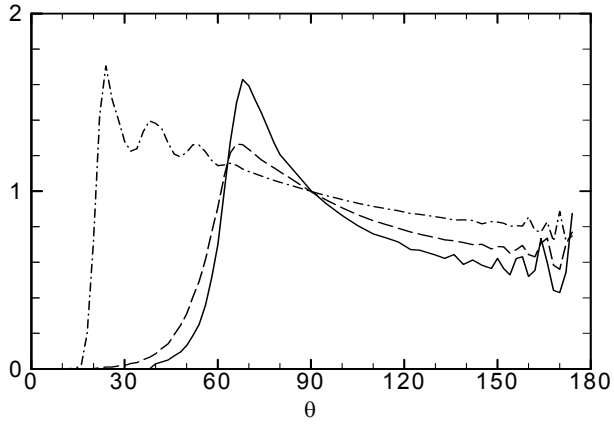

Fig. 9b As figure 8a but for a convecting ring source at observer St = 1.0.

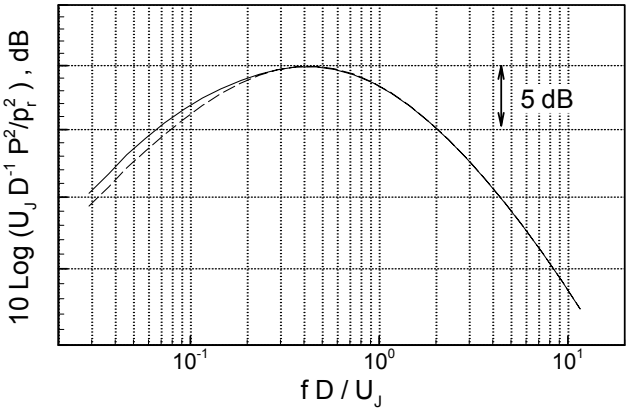

Fig. 10 Far field 90° spectrum for Mach 0.801, T_r =3.0 jet. Exact Green's function (solid line); density-scaled GF (dashed line).

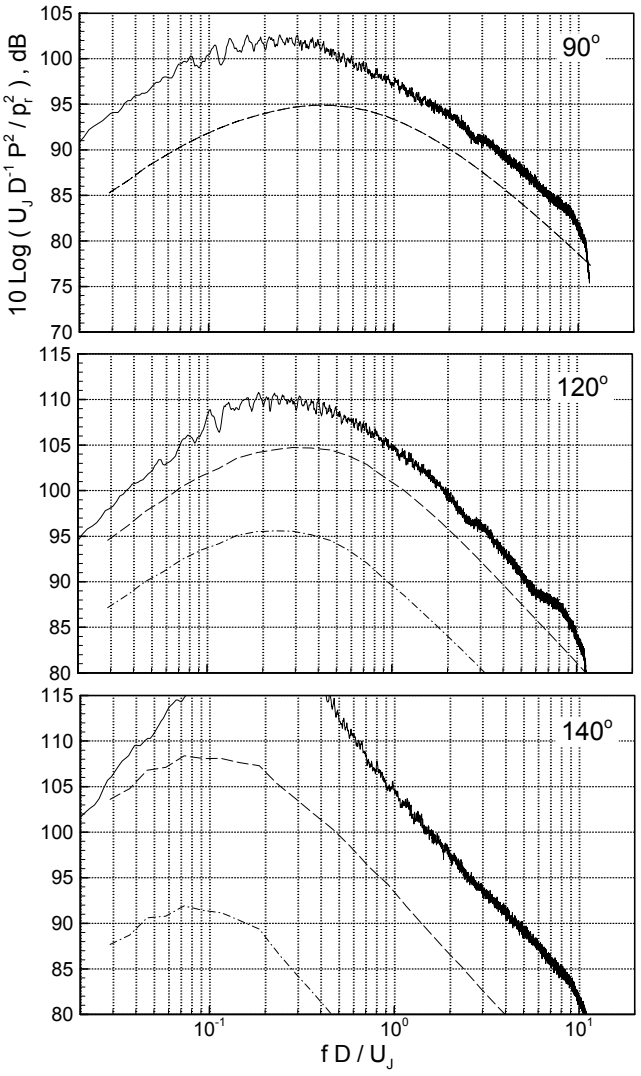

Fig. 11 Far field spectra for Mach 0.801, T_r =3.0 jet at indicated inlet angles and at R/D = 100. Self noise (dash-dot); Self + Shear noise (dashed line); data (solid line).

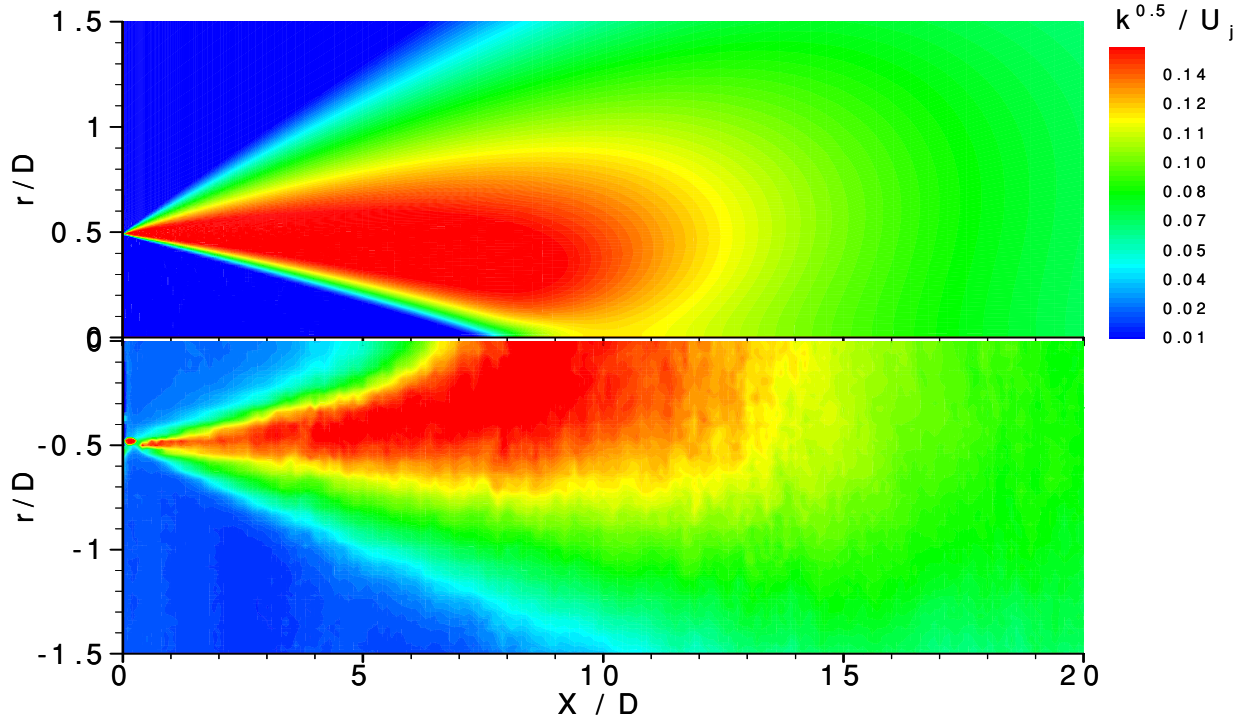

Fig. 12a Distribution of turbulence kinetic energy. Top, RANS prediction for Mach 0.801, T_r = 3.0 hot jet; bottom, PIV measurements for Mach 0.90, T_r = 3.14 hot jet.

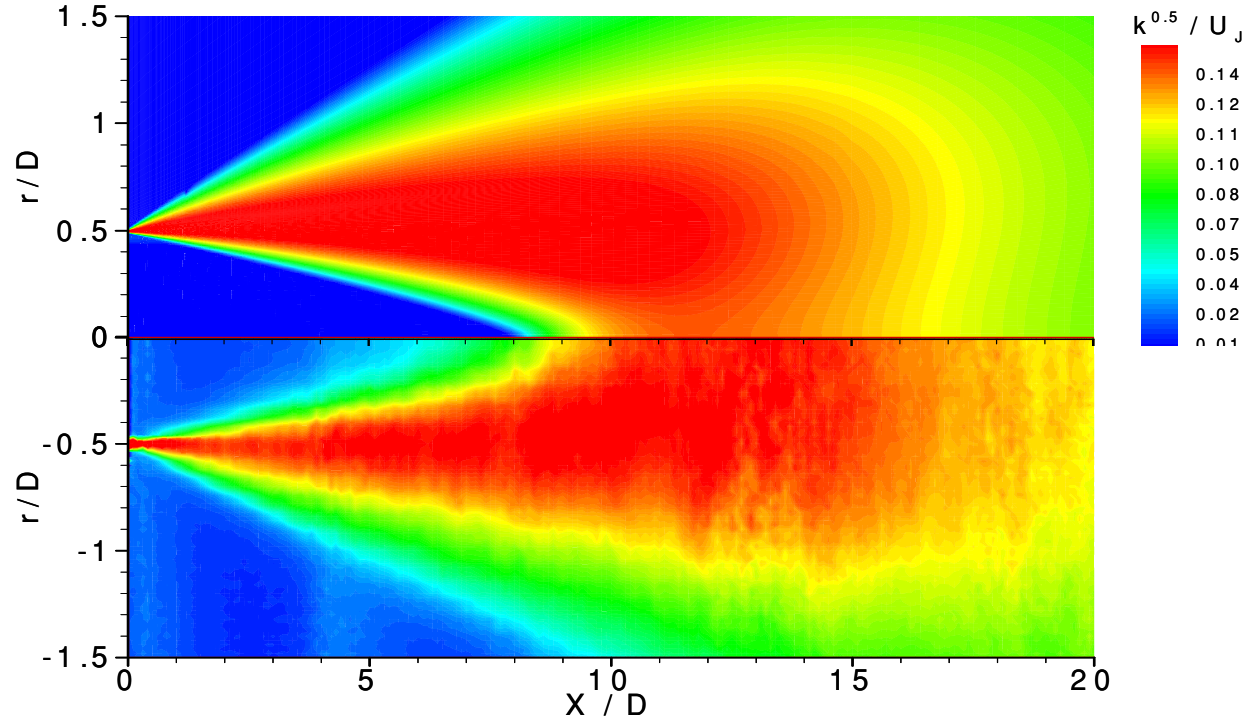

Fig. 12b Distribution of turbulence kinetic energy. Top, RANS prediction for Mach 0.90, T_r = 1.0 jet; bottom, PIV measurements for Mach 0.98, T_r = 1.0 jet.

REPORT DOCUMENTATION PAGE

Form Approved
OMB No. 0704-0188

1. AGENCY USE ONLY (*Leave blank*)	2. REPORT DATE	3. REPORT TYPE AND DATES COVERED
	June 2004	Technical Memorandum

4. TITLE AND SUBTITLE

Modeling of Turbulence Generated Noise in Jets

5. FUNDING NUMBERS

WBS–22–781–30–09

6. AUTHOR(S)

Abbas Khavaran and James Bridges

7. PERFORMING ORGANIZATION NAME(S) AND ADDRESS(ES)

National Aeronautics and Space Administration
John H. Glenn Research Center at Lewis Field
Cleveland, Ohio 44135–3191

8. PERFORMING ORGANIZATION REPORT NUMBER

E–14580

9. SPONSORING/MONITORING AGENCY NAME(S) AND ADDRESS(ES)

National Aeronautics and Space Administration
Washington, DC 20546–0001

10. SPONSORING/MONITORING AGENCY REPORT NUMBER

NASA TM—2004-213105
AIAA–2004–2983

11. SUPPLEMENTARY NOTES

Prepared for the Tenth Aeroacoustics Conference cosponsored by the American Institute of Aeronautics and Astronautics and the Confederation of European Aerospace Societies, Manchester, United Kingdom, May 10–12, 2004. Abbas Khavaran, QSS Group, Inc., 21000 Brookpark Road, Cleveland, Ohio 44135; and James Bridges, NASA Glenn Research Center. Responsible person, Abbas Khavaran, organization code 5940, 216–977–1120.

12a. DISTRIBUTION/AVAILABILITY STATEMENT

Unclassified - Unlimited
Subject Categories: 02 and 71 Distribution: Nonstandard

Available electronically at http://gltrs.grc.nasa.gov

This publication is available from the NASA Center for AeroSpace Information, 301–621–0390.

12b. DISTRIBUTION CODE

13. ABSTRACT ***(Maximum 200 words)***

A numerically calculated Green's function is used to predict jet noise spectrum and its far-field directivity. A linearized form of Lilley's equation governs the non-causal Green's function of interest, with the non-linear terms on the right hand side identified as the source. In this paper, contributions from the so-called self- and shear-noise source terms will be discussed. A Reynolds-averaged Navier-Stokes solution yields the required mean flow as well as time- and length-scales of a noise-generating turbulent eddy. A non-compact source, with exponential temporal and spatial functions, is used to describe the turbulence velocity correlation tensors. It is shown that while an exact non-causal Green's function accurately predicts the observed shift in the location of the spectrum peak with angle as well as the angularity of sound at moderate Mach numbers, at high subsonic and supersonic acoustic Mach numbers the polar directivity of radiated sound is not entirely captured by this Green's function. Results presented for Mach 0.5 and 0.9 isothermal jets, as well as a Mach 0.8 hot jet conclude that near the peak radiation angle a different source/Green's function convolution integral may be required in order to capture the peak observed directivity of jet noise.

14. SUBJECT TERMS	15. NUMBER OF PAGES
Noise; Jet noise; Propulsion noise	23
	16. PRICE CODE

17. SECURITY CLASSIFICATION OF REPORT	18. SECURITY CLASSIFICATION OF THIS PAGE	19. SECURITY CLASSIFICATION OF ABSTRACT	20. LIMITATION OF ABSTRACT
Unclassified	Unclassified	Unclassified	